

Soft Matter

Accepted Manuscript



This is an *Accepted Manuscript*, which has been through the Royal Society of Chemistry peer review process and has been accepted for publication.

Accepted Manuscripts are published online shortly after acceptance, before technical editing, formatting and proof reading. Using this free service, authors can make their results available to the community, in citable form, before we publish the edited article. We will replace this *Accepted Manuscript* with the edited and formatted *Advance Article* as soon as it is available.

You can find more information about *Accepted Manuscripts* in the [Information for Authors](#).

Please note that technical editing may introduce minor changes to the text and/or graphics, which may alter content. The journal's standard [Terms & Conditions](#) and the [Ethical guidelines](#) still apply. In no event shall the Royal Society of Chemistry be held responsible for any errors or omissions in this *Accepted Manuscript* or any consequences arising from the use of any information it contains.

Amyloid- β_{25-35} Peptides Aggregate Into Cross- β Sheets in Unsaturated Anionic Lipid Membranes at High Peptide Concentrations

Jennifer Tang,¹ Richard J. Alsop,¹ Matilda Backholm,¹ Hannah Dies,¹ An-Chang Shi,¹ and Maikel C. Rheinstädter^{1,*}

¹*Department of Physics and Astronomy, McMaster University, Hamilton, Ontario, Canada*

(Dated: January 30, 2016)

One of the hallmarks of Alzheimer's disease is the formation of protein plaques in the brain, which mainly consist of amyloid- β peptides of different length. While the role of these plaques in the pathology of the disease is not clear, the mechanism behind peptide aggregation is a topic of intense research and discussion. Because of their simplicity, synthetic membranes are promising model systems to identify the elementary processes involved. We prepared unsaturated zwitterionic/anionic lipid membranes made of 1-palmitoyl-2-oleoyl-*sn*-glycero-phosphocholine (POPC) and 1,2-dimyristoyl-*sn*-glycero-3-phospho-L-serine (DMPS) at concentrations of POPC/3 mol% DMPS containing 0 mol%, 3 mol%, 10 mol% and 20 mol% amyloid- β_{25-35} peptides. Membrane-embedded peptide clusters were observed at peptide concentrations of 10 and 20 mol% with a typical cluster size of $\sim 11 \mu\text{m}$. Cluster density increased with peptide concentration from $59 (\pm 3)$ clusters/ mm^2 to $920 (\pm 64)$ clusters/ mm^2 , respectively. While monomeric peptides take an α -helical state when embedded in lipid bilayers at low peptide concentrations, the peptides in peptide clusters were found to form cross- β sheets and showed the characteristic pattern in X-ray experiments. The presence of the peptides was accompanied by an elastic distortion of the bilayers, which can induce a long range interaction between the peptides. The experimentally observed cluster patterns agree well with Monte Carlo simulations of long-range interacting peptides. This interaction may be the fundamental process behind cross- β sheet formation in membranes and these sheets may serve as seeds for further growth into amyloid fibrils.

Keywords: amyloid- β peptides, anionic lipid membranes, amyloid aggregates, cross- β sheet motif, X-ray diffraction, synthetic membranes, membrane mediated interaction, membrane distortions, long-ranged peptide interaction

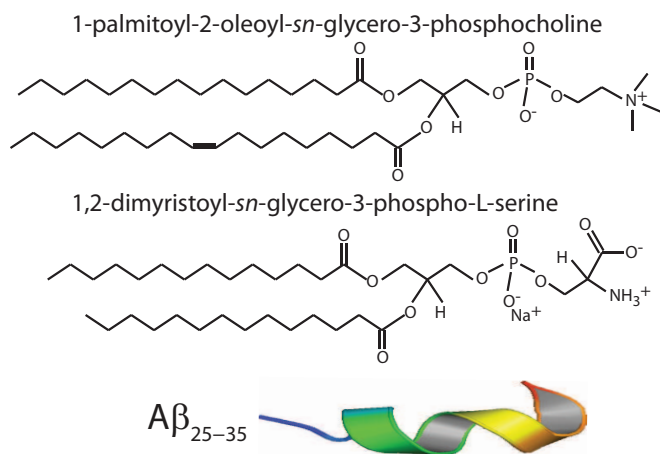


FIG. 1. Schematic representations of POPC, DMPS and Amyloid- β_{25-35} molecules.

1. INTRODUCTION

A primary feature in the pathogenesis of Alzheimer's disease is the deposition of insoluble fibrillar plaques

in the extracellular space of brain tissue [1]. The major component of these plaques is the amyloid- β peptide ($A\beta$). Misfolding and aggregation of $A\beta$ peptides is involved in the development of Alzheimer's disease, although the exact relationship between the protein structure and the pathology of Alzheimer's is still unclear [2]. One stream of anti-Alzheimer's drugs directly addresses amyloid fibres to prevent their formation [3], growth [4] or reduce their toxicity [5]. While the aggregation of proteins appears to be to some extent an inherent part of aging [6], increasing evidence suggests a link between the neurodegenerative disease and changes in the composition of brain tissue.

The $A\beta_{25-35}$ peptide comprises the transmembrane segment of the amyloid precursor protein (APP) and also comprises part of the full length $A\beta_{1-42}$ polypeptide with 42 amino acids. Amyloid fibres are elongated protein structures, consisting of arrays of β -sheets running parallel to the long axis of the fibrils, the so-called cross- β motif [7] connected through steric zippers [1]. It is believed that these fibres need a nucleus to form [8].

While $A\beta$ peptides are frequently reported in an extracellular location, $A\beta_{1-40}$ and $A\beta_{1-42}$ molecules were found to strongly interact with negatively charged lipids and to bind to anionic, negatively charged membranes [9–16], orienting parallel to the membrane surface. Through X-ray and neutron diffraction, Mason *et al.* [17], Dies *et al.* [18] and Dante, Hauf and Dencher [19–21] observed embedded states for $A\beta_{1-42}$ and the $A\beta_{25-35}$ segment in anionic lipid membranes. Both peptides were found to

* Department of Physics and Astronomy, McMaster University, ABB-241, 1280 Main Street West, Hamilton, Ontario L8S 4M1, Canada; Phone: +1-(905)-525-9140-23134, Fax: +1-(905)-546-1252, E-mail: rheinstadter@mcmaster.ca

42 embed as α -helical monomers at low peptide concentra-
43 tions of 3 mol% [12, 18].

44 Van der Waals and electrostatic interactions over long
45 distances alone are typically too weak to overcome ther-
46 mal fluctuations and cause peptides to aggregate. How-
47 ever, when embedded in a membrane, the physical prop-
48 erties of the lipid bilayer contribute to how peptides inter-
49 act. The inclusion of peptides often leads to local distor-
50 tions in membranes, which can interact with each other
51 and lead to repulsive or attractive forces [22–26]. As
52 these forces are mediated by the membrane, they strongly
53 depend on the membrane environment.

54 The membrane active segment amyloid- β_{25-35} was in-
55 cluded in anionic synthetic bilayers at molar concentra-
56 tions of 3 mol%, 10 mol% and 20 mol% and the resulting
57 structures were studied using optical microscopy and X-
58 ray diffraction. Micrometer sized membrane-embedded
59 peptide aggregates were observed at concentrations of
60 more than 10 mol%, showing the characteristic diffrac-
61 tion pattern of cross- β sheets. Cluster formation in-
62 side the bilayers was accompanied by structural changes
63 in the bilayers and local distortions. These distortions
64 can lead to long-ranged peptide-peptide interactions and
65 monte carlo simulations including long-range interactions
66 reproduce the experimentally observed peptide cluster
67 patterns. These aggregates may serve as nuclei for ex-
68 tracelluar plaque growth and we suggest that the corre-
69 sponding distortion driven aggregation process is one of
70 the fundamental mechanisms for nuclei formation.

71 2. MATERIALS AND METHODS

72 2.1. Preparation of the Highly-Oriented 73 Multi-Lamellar Membrane Samples

74 Highly oriented multi-lamellar membranes were pre-
75 pared on single-side polished silicon wafers. 100 mm di-
76 ameter, 300 μm thick silicon (100) wafers were pre-cut
77 into $1 \times 1 \text{ cm}^2$ chips. The wafers were first pretreated
78 by sonication in dichloromethane (DCM) at 310 K for
79 30 minutes to remove all organic contamination and
80 leave the substrates in a hydrophilic state. Each wafer
81 was thoroughly rinsed three times by alternating with
82 $\sim 50 \text{ mL}$ of ultrapure water and methanol.

83 Solutions of 1-palmitoyl-2-oleoyl-*sn*-glycero-3-
84 phosphocholine (POPC) at a concentration of 20 mg
85 of lipid per mL of solvent and 1,2-dimyristoyl-*sn*-
86 glycero-3-phospho-L-serine (DMPS) at a concentration
87 of 10 mg of lipid per solvent were each dissolved in a
88 1:1 chloroform:2,2,2-trifluoroethanol (TFE) solution.
89 The amyloid- β peptides were prepared by pretreatment
90 with trifluoroacetic acid (TFA) to disaggregate the
91 peptide, as described by [27]. This pretreatment
92 included dissolving the peptide in a 1 mg/ml solution
93 of TFA, sonicating with a tip sonicator for four three
94 second intervals, and then removing the solvent through
95 evaporation for 12 hours in a vacuum at 298 K. The

96 peptide was then redissolved in a 20 mg/ml solution of
97 1:1 TFE:chloroform. Each solution underwent several
98 centrifugations in a Vortex mixer several times until
99 the solution was homogeneous. The POPC, DMPS,
100 and peptide solutions were then mixed in appropriate
101 ratios to produce the desired membrane samples for
102 the experiment. Schematics of the POPC, DMPS and
103 $A\beta_{25-35}$ molecules are shown in Figure 1.

104 The tilting incubator (VWR Incubating Rocker/3-D
105 Rotator Waver) was heated to 313 K and the lipid so-
106 lutions were placed inside to equilibrate. 65 μL of lipid
107 solution was applied on each wafer, and the solvent was
108 then allowed to slowly evaporate for 10 minutes at a
109 speed of 15, tilt of 1, such that the lipid solution spread
110 evenly on the wafers. After drying, the samples were
111 placed in vacuum at 313 K for 12 hours to remove all
112 traces of the solvent. The bilayers were annealed and re-
113 hydrated before use in a saturated K_2SO_4 solution which
114 provides $\sim 97\%$ relative humidity (RH). The hydration
115 container was allowed to equilibrate at 293 K in an in-
116 cubator. The temperature of the incubator was then in-
117 creased gradually from 293 K to 303 K over a period of
118 ~ 5 hours to slowly anneal the multi-lamellar structure.
119 This procedure results in highly oriented multi-lamellar
120 membrane stacks and a uniform coverage of the silicon
121 substrates. About 3,000 highly oriented stacked mem-
122 branes with a thickness of $\sim 10 \mu\text{m}$ are produced using
123 this protocol.

124 The high sample quality and high degree of order is a
125 prerequisite to determine in-plane and out-of-plane struc-
126 ture of the membranes separately, but simultaneously.
127 Table 2 lists all samples prepared for this study.

128 2.2. Inverted Light Microscope

129 Optical microscopy in this study was performed us-
130 ing an Olympus BX51 microscope. Samples were im-
131 aged in dark field reflection mode with a CCD camera
132 (QIClick, QImaging), which provided high resolution im-
133 ages (1392×1040 pixels) for subsequent image analysis.
134 In dark field microscopy, the unscattered beam is ex-
135 cluded from the image by illuminating the sample with
136 light that when reflected will not be collected by the ob-
137 jective lens. A $50\times$ magnification objective (UMPlanFI,
138 Olympus) was used to obtain images with a resolution of
139 130 nm/pixel. Additional images with lower resolution
140 were taken using a Nikon P520 digital camera in high-
141 resolution macro setting mode.

142 2.3. X-ray Scattering Experiment

143 X-ray diffraction data was obtained using the Biologi-
144 cal Large Angle Diffraction Experiment (BLADE) in the
145 Laboratory for Membrane and Protein Dynamics at Mc-
146 Master University. BLADE uses a 9 kW (45 kV, 200 mA)
147 $\text{CuK}\alpha$ Rigaku Smartlab rotating anode at a wavelength

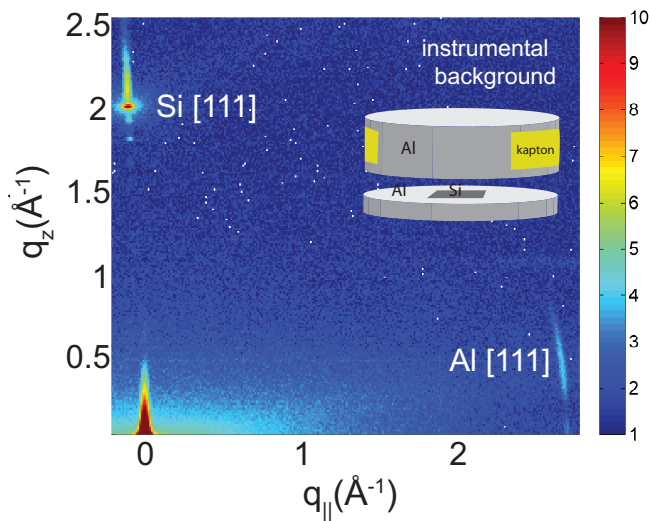


FIG. 2. Background signals of the pure silicon wafer show the [111] reflection normal to the wafer. The aluminum [111] reflection is observed in the plane of the wafers as contribution from the sample can.

148 of 1.5418 Å. Both source and detector are mounted on
 149 movable arms such that the membranes stay horizontal
 150 during the measurements. Focussing multi-layer optics
 151 provides a high intensity parallel beam with monochro-
 152 matic X-ray intensities up to 10^{10} counts/(s×mm²). This
 153 beam geometry provides optimal illumination of the solid
 154 supported membrane samples to maximize the scatter-
 155 ing signal. By using highly oriented membrane stacks,
 156 the in-plane ($q_{||}$) and out-of-plane (q_z) structure of the
 157 membranes can be determined separately but simultane-
 158 ously.

159 The result of such an X-ray experiment is a 2-
 160 dimensional intensity map of a large area ($0.03 \text{ \AA}^{-1} <$
 161 $q_z < 1.1 \text{ \AA}^{-1}$ and $0 \text{ \AA}^{-1} < q_{||} < 3.1 \text{ \AA}^{-1}$) of the recip-
 162 rocal space. The corresponding real-space length scales
 163 are determined by $d = 2\pi/|Q|$ and cover length scales
 164 from about 2.5 to 60 Å, incorporating typical molecular
 165 dimensions and distances. These 2-dimensional data are
 166 essential to detect and identify signals from bilayers and
 167 peptides and determine orientation of the molecules. All
 168 scans were carried at 28°C and 97% RH. The membrane
 169 samples were mounted in a temperature and humidity
 170 controlled chamber, a so-called humidity chamber, dur-
 171 ing the measurements. The membranes were hydrated
 172 by water vapour and allowed to equilibrate for 6 hours
 173 before the measurements to ensure full re-hydration of
 174 the membrane stacks.

175 In order to unambiguously determine the small peptide
 176 signals the experimental background was measured and
 177 it shown in Figure 2. The 2-dimensional data show con-
 178 tributions of the silicon wafer, the [111] reflection normal
 179 to the wafer, and the aluminium [111] reflection in the
 180 plane as contribution from the sample can. The wafers
 181 used were cut such that the strong [111] silicon reflection

Simulation parameter	Value
lipid-lipid	-0.5 $k_B T$
peptide-peptide	-1.5 $k_B T$
lipid-peptide	-
too-close-distance	1.5
interaction distance	1.5-20

TABLE 1. Simulation details. Simulations were implemented in NetLogo. The simulation box contained 2,000 particles.

182 is not perfectly perpendicular to the surface of the wafers
 183 to avoid overlap with the membrane and peptide signals.

184 The degree of orientation of the bilayers and lipid tails
 185 within the membrane samples was determined from the
 186 2-dimensional X-ray maps. The intensity as a function of
 187 of Q and angle γ from the $q_{||}$ axis was used to determine
 188 orientation of lipid tail signals. Pixels within a wedge of
 189 the reciprocal space map, defined by γ and γ_{step} (where
 190 $\gamma_{step} = 2^\circ$), were integrated as a function of $Q = (q_z^2 +$
 191 $q_{||}^2)^{1/2}$ and normalized by pixel count at each Q . γ varied
 192 from 10° to 35° for samples with 0 mol%, 3 mol%, and
 193 10 mol% peptide and from 10° to 85° for the sample with
 194 20 mol% peptide. $\gamma < 10^\circ$ was not included due to high
 195 absorption at low angles [28]. The integrated $I(Q, \gamma)$
 196 could be fit with Lorentzian functions. By calculating
 197 the area under the Lorentzian fits, $I(\gamma)$ was determined
 198 and fit with a Gaussian distribution.

199 To determine the degree of orientation of membranes
 200 in the stack, the intensity as a function of the meridional
 201 angle δ was determined. The intensity was integrated
 202 around the second Bragg peak, at $Q \approx 0.22 \text{ \AA}^{-1}$, from
 203 $18^\circ < \delta < 40^\circ$. $\delta < 18^\circ$ was not used in order to avoid
 204 contributions from incoherent scattering [29]. The second
 205 Bragg peak was chosen as incoherent contributions were
 206 weaker than the first Bragg peak. Pixel density at low-
 207 Q was too low to calculate $I(Q, \delta)$ as with the peptide
 208 samples, so $I(\delta)$ was calculated by direct summation of
 209 pixels within δ and δ_{step} (where $\delta_{step} = 2^\circ$), and within Q
 210 and Q_{step} , where the Q -range was chosen to include only
 211 scattering from the second Bragg peak. $I(\delta)$ was fit with
 212 a Gaussian distribution centred at $\delta=0$, which was then
 213 used to calculate the degree of orientation using Hermans
 214 orientation function:

$$f = \frac{3 \langle \cos^2 \delta \rangle - 1}{2}. \quad (1)$$

2.4. Monte Carlo Simulations

216 The simulation was implemented in the multiagent
 217 NetLogo environment [30, 31]. The simulation box con-
 218 tained 2,000 lipid molecules and peptides at concentra-
 219 tions of 0%, 3%, 10% and 20%, in agreement with the
 220 experiment. The lipid bilayer was modelled by an at-
 221 tractive lipid-lipid force of -0.5 $k_B T$. An attractive force
 222 between peptides of -1.5 $k_B T$ was implemented, whose in-
 223 teraction distance could be varied from a direct peptide-

224 peptide interaction to a long-range interaction over 20
 225 nearest neighbour distances. The parameters of the sim-
 226 ulation are listed in Table 1. All simulations started at a
 227 random configuration and were run for 20,000 time steps
 228 to ensure that they reach equilibrium.

229 3. RESULTS

230 Anionic lipid membranes were prepared with 97 mol%
 231 1-palmitoyl-2-oleoyl-*sn*-glycero-phosphocholine (POPC),
 232 a 16:0-18:1 zwitterionic phospholipid with one saturated
 233 and one unsaturated tail, and 3 mol% 1,2-dimyristol-
 234 *sn*-glycero-3-phospho-L-serine (DMPS), a 14 chain fully
 235 saturated anionic phospholipid. A small percentage of
 236 charged phospholipids is found in cell membranes in the
 237 brain and is essential for proper cell signalling, protein
 238 sorting, and cell adhesion [32]. Four different membrane
 239 complexes were prepared for this study, as detailed in the
 240 Materials and Methods Section and listed in Table 2.

242 The results section is organized as follows: Size distri-
 243 bution and density of the peptide aggregates were deter-
 244 mined from optical microscopy. From intensity and dis-
 245 tribution of membrane and peptide signals in high res-
 246 olution X-ray diffraction experiments, molecular struc-
 247 ture of the peptide aggregates and effect of the peptides
 248 on bilayer structure was determined and a model for
 249 cluster structure developed. The effect of local bilayer
 250 distortions on peptide-peptide interactions was studied
 251 through long-ranged peptide interactions in monte carlo
 252 computer simulations.

253 3.1. Optical Microscopy

254 Microscope images of POPC/DMPS bilayers at (a)
 255 0 mol% $A\beta_{25-35}$ and (b) 20 mol% $A\beta_{25-35}$ are shown
 256 in Figure 3. The pure lipid bilayer in part (a) shows a
 257 smooth and aggregate free surface. No peptide aggre-
 258 gates were observed at 3 mol% peptides. At 10 mol%
 259 $A\beta_{25-35}$, almost circular structures become visible whose
 260 density increases at 20 mol% peptide, as shown in part
 261 (b). Number and size of these structures were deter-
 262 mined by analyzing several images at each concentration
 263 taken at different spots of the solid supported membrane
 264 stacks.

265 The corresponding histograms are shown in Figure 4.
 266 A normal distribution was fit and size of the clusters
 267 was determined to be $11.0 \pm 1.1 \mu\text{m}$ for 10 mol% and
 268 $10.9 \pm 2.5 \mu\text{m}$ for 20 mol%. While the size of clusters
 269 stayed approximately constant between 10 and 20 mol%,
 270 the density of clusters increased from $59 \pm 3 \text{ mm}^{-2}$ to
 271 $920 \pm 64 \text{ mm}^{-2}$.

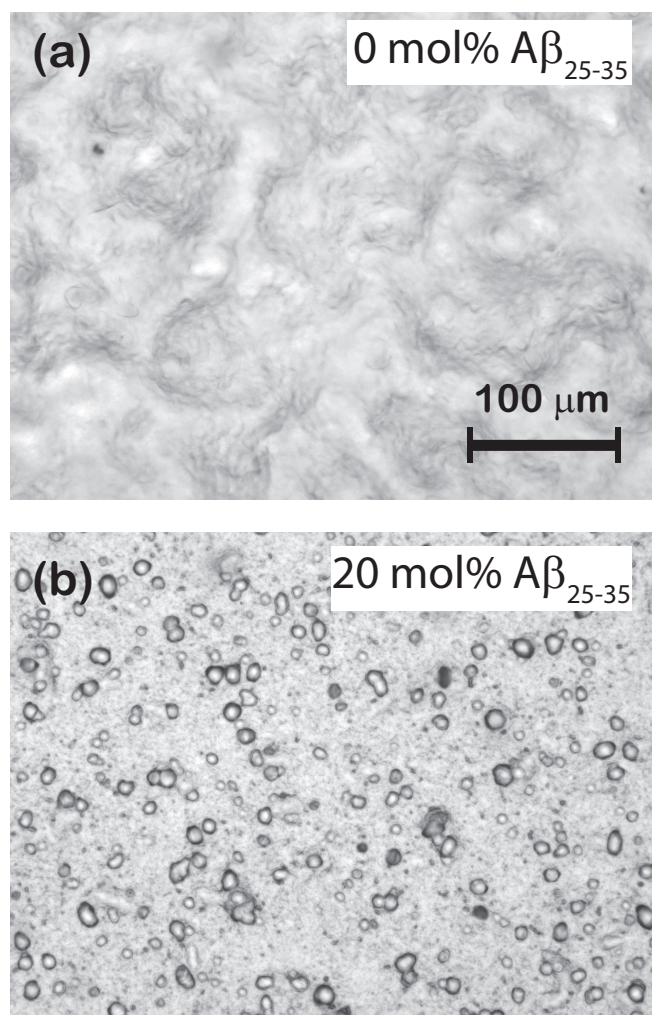


FIG. 3. Optical microscopy images of a (a) pure POPC/DMPS membrane and (b) a POPC/DMPS+20 mol% $A\beta_{25-35}$. While the pure lipid matrix shows a smooth surface, inclusions were observed at peptide concentrations of 10 and 20 mol%.

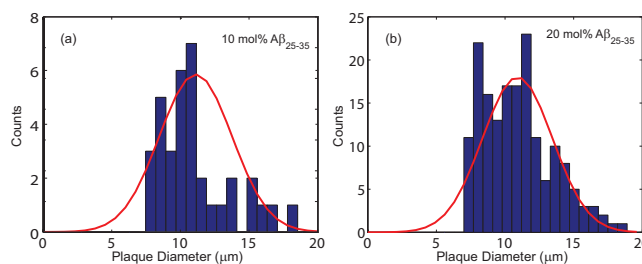


FIG. 4. Histograms of the cluster size distribution in bilayers containing (a) 10 mol% $A\beta_{25-35}$ and (b) 20 mol% $A\beta_{25-35}$. The cluster sizes were determined from normal distributions to be $11.0 \pm 1.1 \mu\text{m}$ and $10.9 \pm 2.5 \mu\text{m}$ with cluster densities of 59 ± 3 and $920 \pm 64 \text{ clusters/mm}^2$, respectively.

$A\beta_{25-35}$ (mol%)	d_z (Å)	d_{HH} (Å)	d_{water} (Å)	a_T (Å)	Δa_T (Å)	A_T (Å ²)	V_T (Å ³)	f Membranes	lipid tail tilt (°)
0	59.0±0.1	39.4±1.0	19.6±0.5	5.20±0.05	0.59±0.02	23.4±0.1	922±1	0.96±0.02	19.2±5
3	54.9±0.1	39.1±1.0	15.8±0.4	5.21±0.05	0.61±0.02	23.5±0.1	919±1	0.92±0.03	21.4±2.3
10	61.6±0.4	39.2±1.0	22.4±0.6	5.21±0.05	0.67±0.02	23.5±0.1	921±1	0.90±0.03	20.5±2.3
20	58.0±0.2	39.3±1.0	18.7±0.5	5.06±0.05	0.74±0.02	22.6±0.1	886±1	0.86±0.03	25.4±3

TABLE 2. Structural parameters for the different amyloid- β_{25-35} concentrations. While the lamellar d_z -spacing changes with peptide concentration, the head group-head group distance d_{HH} stays constant such that changes can be attributed to the water layer thickness, d_{water} . Distance between acyl chains (a_T), area per tail (A_T) and tail volume (V_T) continuously decrease with increasing peptide concentration while the disorder in tail packing increases (Δa_T). The membrane orientation parameter, f , decreases and lipid tilt angles increase, indicating and increasing distortion of the bilayers with increasing peptides concentration.

272

3.2. X-ray Diffraction

273 The multi-lamellar membrane complexes were oriented
274 in the diffractometer such that the $q_{||}$ axis probed lat-
275 eral membrane structure and the perpendicular axis, q_z ,
276 probed out-of-plane structure. The samples were kept in
277 a temperature and humidity controlled chamber during
278 the measurements. Data were collected at $T = 28^\circ\text{C}$ and
279 in a 97% H_2O atmosphere to ensure full hydration of the
280 membranes to study structure in the fluid, physiologically
281 relevant fluid state.

282 Figures 5 (a)-(d) show 2-dimensional X-ray intensity
283 maps for (a) POPC/DMPS, (b) POPC/DMPS+3 mol%
284 $A\beta_{25-35}$ and , (c) POPC/DMPS+10 mol% $A\beta_{25-35}$ and
285 , (d) POPC/DMPS+20 mol% $A\beta_{25-35}$. The out-of-plane
286 scattering along q_z shows pronounced and equally spaced
287 Bragg intensities due to the multi-lamellar structure of
288 the membranes, as reviewed for instance in [33, 34].

289 The diffracted intensity shows a well developed in-
290 plane Bragg feature along the $q_{||}$ -axis at $q_{||} \sim 1.4 \text{ \AA}^{-1}$,
291 related to the packing of the lipid tails in the hydropho-
292 bic membrane core. This peak is the result of a hexag-
293 onal packing of lipid tails [35] (planar group p6). The
294 distance between two acyl tails is determined to be
295 $a_T = 4\pi/(\sqrt{3}q_T)$, where q_T is the position of the tail
296 correlation peak. The area per lipid acyl chain is ob-
297 tained to $A_T = \sqrt{3}/2a_T^2$. Additional features appear at
298 high peptide concentrations.

299 For a quantitative analysis of the diffracted intensi-
300 ties, the 2-dimensional data were cut along the out-of-
301 plane and in-plane axes. Reflectivities for all samples
302 are shown in Figure 6. While 5 Bragg reflections were
303 observed for the pure lipid matrix and at 3 mol% pep-
304 tides, addition of 10 and 20 mol% reduces the number
305 of peaks to 3, indicative of a less well-ordered lamellar
306 structure. The lamellar spacings, d_z , of the membrane
307 complexes, *i.e.*, the distance between two neighbouring
308 bilayers in the membrane stack, was determined from
309 the distance between the well developed Bragg reflections
310 ($d_z = 2\pi/\Delta q_z$). The thickness of the membrane, given
311 by the head group to head group spacing (d_{HH}), and
312 the thickness of the hydration water layer, d_{water} , were
313 determined from electron density distributions through
314 Fourier transformation of the reflectivity data and the re-
315 sults are given in Table 2. While changes were observed

316 in the lamellar spacing d_z upon addition of $A\beta_{25-35}$, the
317 membrane thickness d_{HH} stayed almost constant.

318 In-plane diffraction data are shown in Figure 7. Dif-
319 ferent signals can be assigned, corresponding to different
320 molecular components. A signal from the membrane hy-
321 dration water, *i.e.*, water molecules in the water layer
322 between stacked membranes at 3.4 \AA ($q_{||}=1.85 \text{ \AA}^{-1}$) is
323 observed for all concentrations [36, 37]. We note that the
324 characteristic distance in bulk water is slightly smaller,
325 namely $\sim 3.1 \text{ \AA}$ (2 \AA^{-1}). Due to interactions with the bi-
326 layer, membrane hydration water has distinct properties
327 as compared to bulk water, such as structure, freezing
328 temperature and dynamics [38, 39].

329 The distance between lipid chains can be determined
330 from the position of the acyl chain correlation peak while
331 the width of the peak is related to the packing density
332 in the hydrocarbon core. Values for a_T , Δa_T , the area
333 and the volume per lipid acyl chain are given in Table 2.
334 The chain distance and area continuously decrease with
335 peptide concentration while packing order decreases. The
336 volume occupied by the lipid tails decreases by $\sim 7\%$ upon
337 addition of 20 mol% peptide.

338 Additional narrow signal are observed at $q_{||}$ -values of
339 1.43 and 1.5 \AA^{-1} in the 0 and 3 mol% membranes. These
340 signals have been reported before [40–42] and assigned to
341 the organization of the lipid head groups within the lipid
342 matrix. Peak positions are well described by a rectangu-
343 lar unit cell with dimensions $a = 8.38 \text{ \AA}$ and $b = 8.79 \text{ \AA}$.
344 The corresponding arrangements of lipid tails and head
345 groups are pictured in the cartoon next to the diffraction
346 patterns in Figure 7.

347 Two signals appear with increasing peptide concen-
348 tration. While it has been reported previously that
349 amyloid- β_{25-35} peptides dissolve as monomeric α -helices
350 in anionic membranes at a low peptide concentration of
351 3 mol% [12, 18], the signals at 10 \AA ($q_{||}=0.6 \text{ \AA}^{-1}$) and
352 4.7 \AA ($q_{||}=1.35 \text{ \AA}^{-1}$) are the pattern of amyloid peptides
353 forming cross- β amyloid sheets. These signals are ob-
354 served at 10 mol%, when cluster formation was detected,
355 and increase with increasing peptide concentration.

356 The structure of a cross- β sheet is depicted in Fig-
357 ure 8 (d). The two reflections observed in the X-ray pat-
358 tern correspond to inter-strand and inter-sheet distances
359 of peptide chains. The reflection at 1.35 \AA^{-1} is indicative

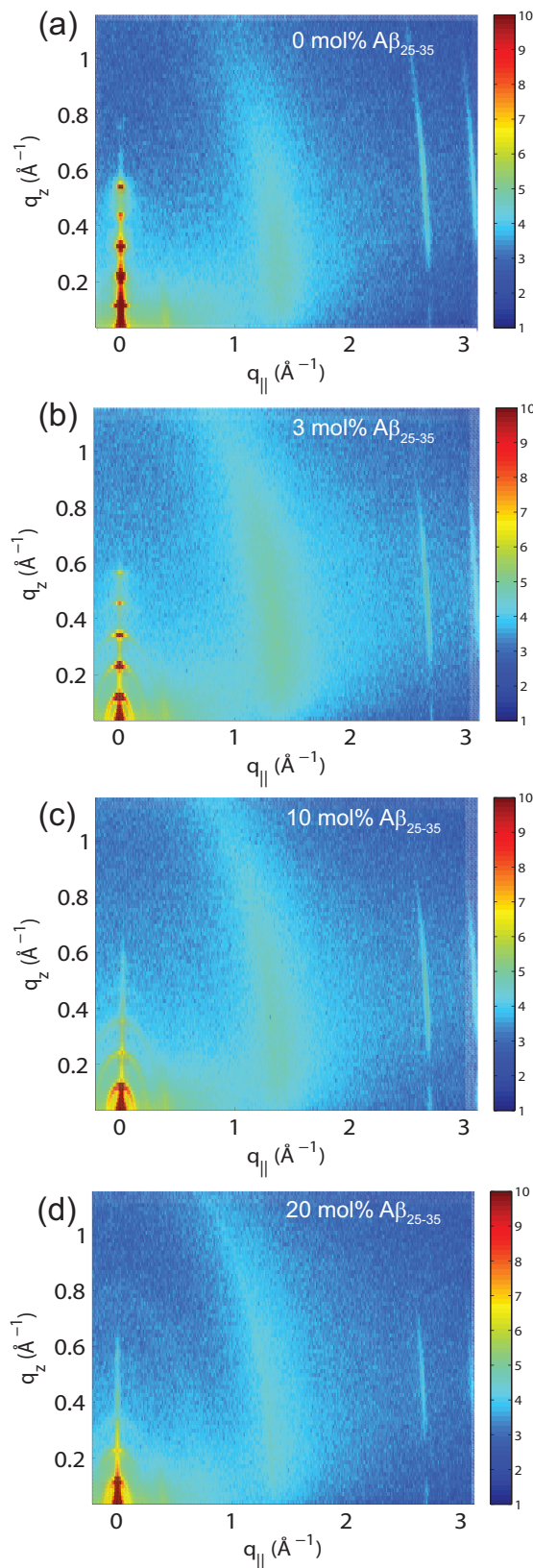


FIG. 5. (a)-(d) 2-dimensional Diagram of the experimental setup used for the X-ray diffraction measurements. Two-dimensional data sets were collected to study molecular structure perpendicular to the solid supported membranes (out-of-plane) and parallel to the membranes (in-plane).

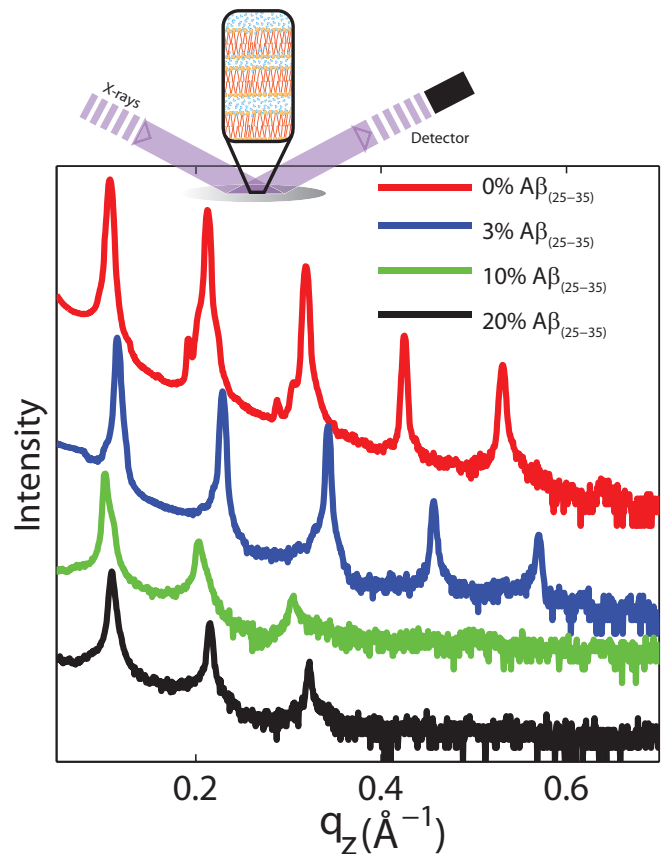


FIG. 6. Out-of-plane diffraction for all membrane complexes. The lamellar structure of the membrane stack leads to a series well defined of Bragg peaks. Five diffraction orders were observed for 0 and 3 mol% $A\beta_{25-35}$, while only 3 lamellar orders are visible for the cluster forming concentrations of 10 and 20 mol% peptide. Lamellar d_z -spacings, head group-head group distances, d_{HH} , and water layer thickness, d_{water} , were determined from this data and are listed in Table 2.

360 of extended protein chains running roughly perpendicular
 361 to the membrane plane and spaced 4.7 Å apart. The
 362 reflection at 0.6 Å⁻¹ shows that the extended chains are
 363 organized into sheets spaced 10 Å apart.

364 These measurements are indicative that amyloid- β
 365 peptides partition in anionic lipid bilayers at high pep-
 366 tide concentrations of 10 and 20 mol% and form cross- β
 367 sheets. Inclusion of the peptides has a profound effect
 368 on the structure of the bilayers: it leads to a reduction
 369 of distance between neighboring chains and a distortion
 370 in chain packing. The interaction between peptides and
 371 bilayers and the role of bilayer distortions will be inves-
 372 tigated further in the next section.

3.3. Angular Distribution of Membrane and Peptide Signals

375 The average orientation of the lipid bilayers and the
 376 tilt of the lipid molecules can be determined by studying

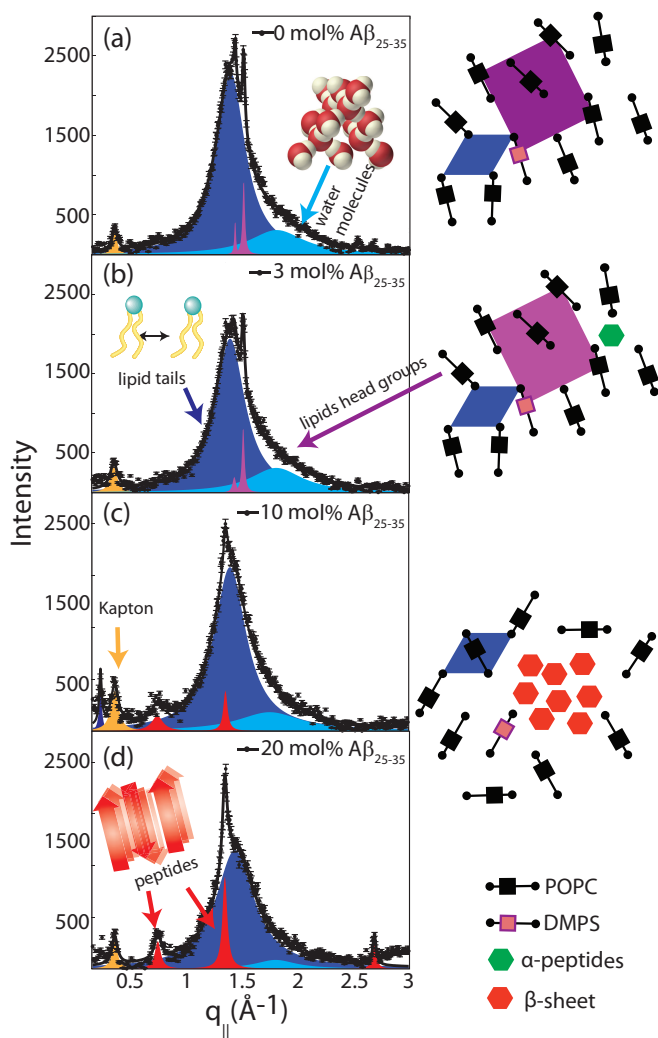


FIG. 7. In-plane X-ray diffraction of the POPC/DMPS lipid membranes at different concentrations of amyloid- β_{25-35} . The signals at 0 and 3 mol% $A\beta$ can be assigned to organization of lipid tails, lipid head groups and hydration water molecules. The corresponding structures are depicted in the cartoons on the right. Peptides occur in monomeric α -helical states at these low peptide concentrations. Signals corresponding to formation of cross- β peptide sheets were observed at peptide concentrations of 10 and 20 mol%. The volume concentration of the different phases is proportional to the integrated intensities of the corresponding correlation peaks. The position, width, and intensity of the peaks are fit by a least-square algorithm. 15 free parameters are varied per fit. The signal at $q_{\parallel}=0.4 \text{ \AA}^{-1}$ is a contribution of the kapton window of the X-ray chamber.

the angular dependence of the corresponding diffraction signals on the 2-dimensional X-ray intensity maps. The pattern for 20 mol% and the assignment of the scattering signals are depicted in Figure 8 (a). The intensity at the lipid tail position was integrated as function of the azimuth, γ , to determine the average tilt angle of the lipid acyl chains.

Figure 8 (b) shows the small angle region around the

reflectivity Bragg peaks in magnification. The corresponding intensity shows a circular pattern and was integrated over the meridian, δ , and analyzed using Hermans orientation function, as detailed in the Materials and Methods Section. Hermans function describes the degree or extent of orientation of the molecular axis relative to the membrane normal. Completely aligned would result in $f=1$, randomly oriented in $f=0$ and a perpendicular orientation would give $f=-0.5$.

For a perfectly ordered membrane stack, where all bilayers are planar and perfectly parallel, the intensity of the reflectivity Bragg peaks is located along the q_z -axis. There are two origins for a smearing of the intensity: The lamellar diffuse scattering occur in horizontal sheets as a result of bilayer undulations. By analyzing this intensity, the elastic constants of the bilayers can be determined [33, 43, 44]. Bilayers, which are bent permanently lead to a ring of intensity on the 2-dimensional plots (a powder ring). This intensity is a measure of the static distortions of the bilayers caused by the presence of the peptides.

Signals of membrane curvature and lipid tails orientation are plotted in Figure 9 and the results are listed in Table 2. Bending of the bilayers and the average tilt angles of the lipid tails increase with peptide concentration, indicative of increasing bilayer distortions in the presence of peptides and peptide aggregates.

3.4. Monte Carlo Modelling

In order to investigate aggregation of peptides and in particular the effect of the range of peptide interaction, Monte Carlo simulations were conducted. The computer modelling results are shown in Figure 10. The system consisted of a planar system of 2,000 lipid and peptide molecules, with peptide concentrations of 3, 10 and 20 mol% peptide. The lipid bilayer was modelled by an attractive lipid-lipid force of $0.5 k_B T$. An attractive peptide-peptide force of $1.5 k_B T$ was included and simulation runs at different interaction distances were conducted for 3 mol%, 10 mol% and 20 mol% $A\beta_{25-35}$ peptides.

A direct peptide-peptide interaction, as modelled at a range of 3 molecular distances, is shown in Figures 10 (a)-(c) and was found to lead to cluster formation at all peptide concentrations. Cluster size increases with peptide concentration, in conflict with the experimental findings. Truly long range interactions over 20 molecular distances (Figures 10 (m)-(o)) were found to suppress cluster formation at low peptide concentrations of 3 mol%, however, also led to an increasing cluster size at higher peptide concentrations.

A peptide-peptide interaction of 10 molecular distances in parts (d)-(f) was found to best reproduce the experimental patterns: (1) there is a threshold, *i.e.*, no clusters form at low peptide concentrations and (2) cluster size is independent of the amount of peptides at higher concen-

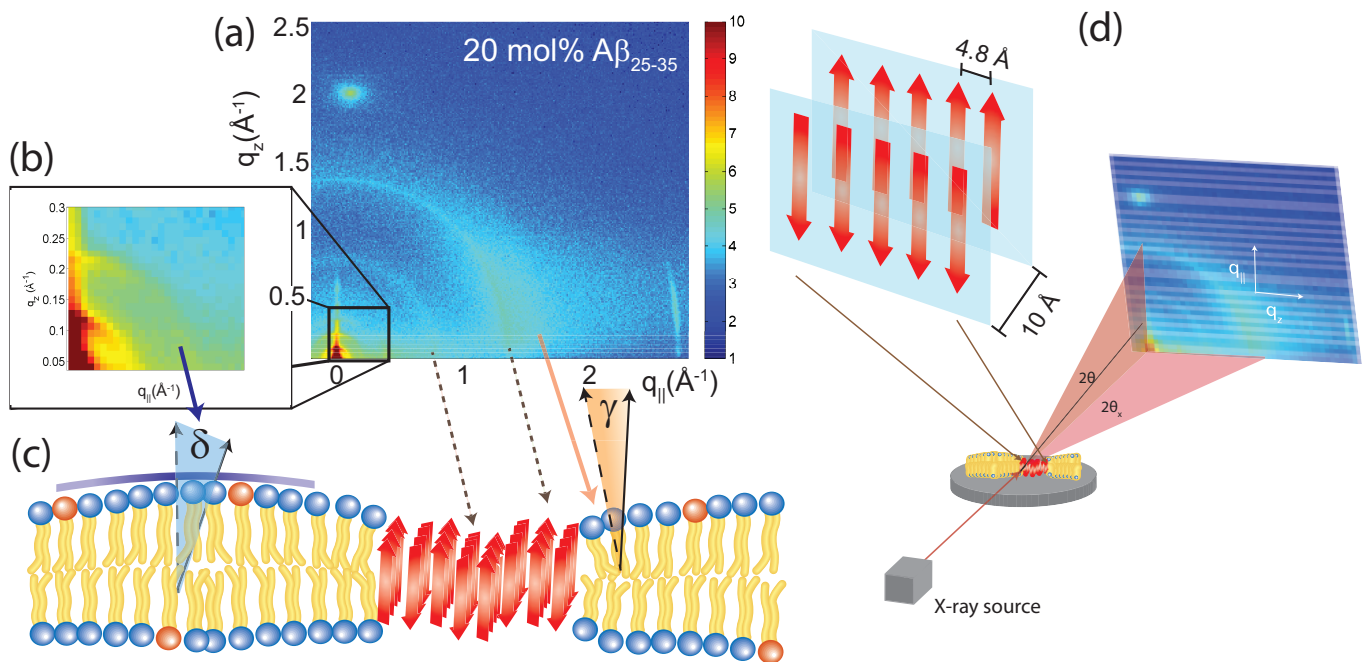


FIG. 8. (a) Two-dimensional X-ray diffraction image of a membrane with 20 mol% $A\beta$ peptides. The various features can be assigned to lipid and peptide structures in the membrane. (b) An inset of the image at low- Q , highlighting the presence of more isotropic scattering and elastic distortions. (c) A model of the cluster in the membrane. Hydrophobic matching by the membranes to the peptide leads to distortions in the membrane structure. (d) Structure of a cross- β sheet. The 4.8 Å distance corresponds to chain distances within a sheet while the 10 Å distance is the distance between antiparallel sheets.

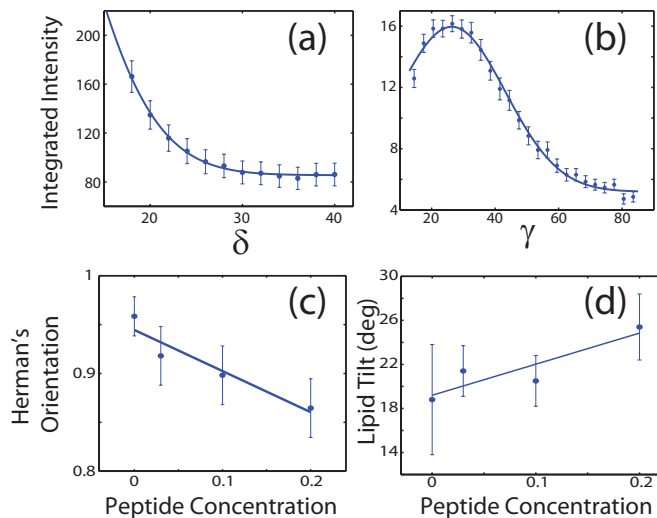


FIG. 9. (a) Intensity of the second reflectivity Bragg peak as a function of angle θ from the q_z axis. (b) Integrated intensity of the lipid correlation peak as a function of angle γ from the $q_{||}$ axis. (c) Hermans orientation function, as defined in the Materials and Methods Section in Equation (1), for membrane bending for all peptide concentrations and (d) lipid tail tilt angle for all peptide concentrations.

4. DISCUSSION

4.1. Effects of peptide insertion and cluster formation on bilayer properties

The structures that we observe in the optical microscopy images in Figure 3 only appear at high levels of the amyloid peptides and go hand-in-hand with the occurrence of beta-peptide signals in the X-ray diffraction experiment in Figures 5 and 7. The intensity of these signals increases with peptide concentration, in agreement with the increase in cluster density in the microscopy images. From the structural parameters of the bilayers in Table 2 there is no significant increase in lamellar spacing in the presence of the peptides such that we can exclude that the peptide clusters form outside of the bilayers. We note that the constant amount of 3mol% DMPS in the POPC/DMPS mixture is too small to explain the occurrence of the observed heterogeneities based on a lipid demixing or change in lipid structure. We, therefore, conclude that the observed structures are embedded in the bilayers and consist of a high concentration of peptides. The structural parameters give a detailed picture of organization and interaction between peptides and peptide clusters and anionic lipid membranes.

With the addition of $A\beta_{25-35}$ peptides to the anionic lipid bilayers (1) the average membrane thickness, as measured by the head group-head group distance d_{HH} , does not change. (2) the distance between acyl chains,

440 trations.

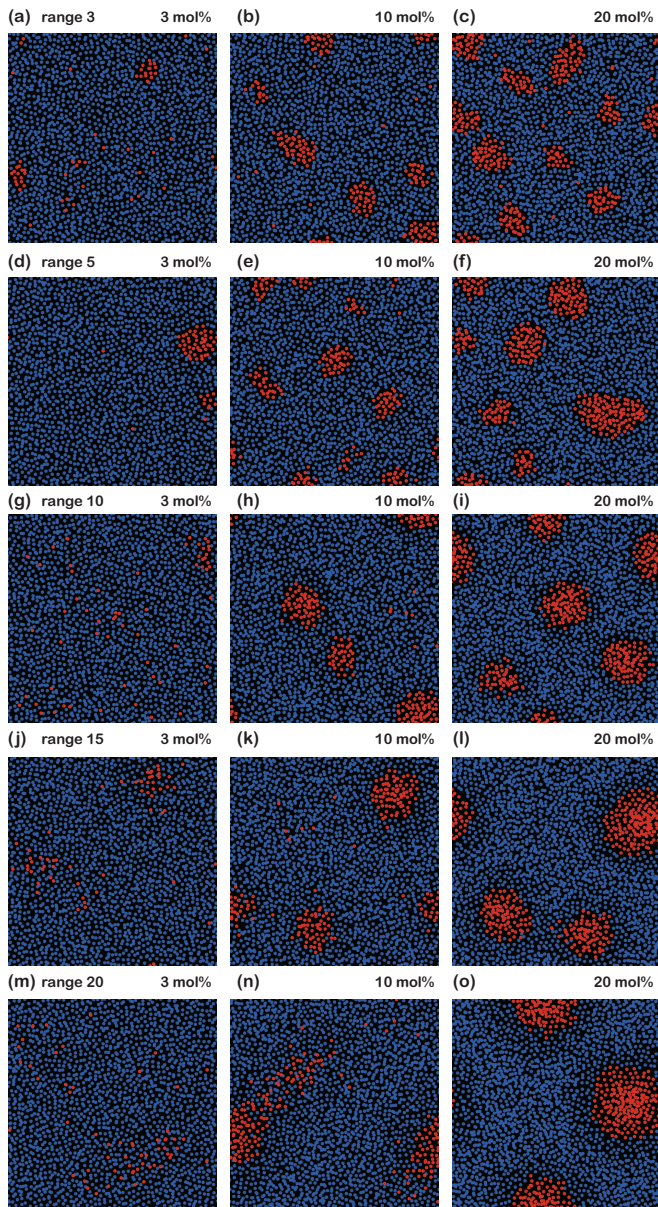


FIG. 10. Monte Carlo Simulations of a lipid bilayer containing different peptide concentrations. A nearest-neighbour interaction between peptides was simulated in (a), (b) and (c). A long-range interaction including up to 20 molecular distances in (d), (e) and (f) was found to best mimic the experimental findings.

the area and volume per lipid tail continuously decrease while the distribution of tail distances increases. In order to accommodate the peptides the (3) average lipid acyl chain tilt increases, lipid tail disorder increases, and membrane orientation parameter decreases, indicative of increasing local distortions. The structure of the bilayer at high peptide concentrations is sketched in Figure 8 (c).

It is expected that membrane-mediated interactions between the inserted proteins play a major role in the aggregation behaviour of the $A\beta_{25-35}$ peptides. In gen-

eral, a number of mechanisms could generate membrane-mediated interactions between the peptides. First of all, the hydrophobic thickness of the transmembrane proteins does not necessarily match the equilibrium bilayer thickness, thus inducing hydrophobic mismatch in the system. The hydrophobic mismatch may induce protein clustering. Secondly, the inserted proteins may lead to localized lateral displacements of the lipids and/or curvature change of the membranes, resulting in local packing interactions. Finally the insertion of proteins could affect the fluctuation modes of the membranes, resulting in Casimir forces between the proteins. In the current system composed the inserted $A\beta_{25-35}$ peptides could be influenced by one or more of these mechanisms, resulting in the clustering of the peptides at high concentrations.

One possible mechanism involves the local deformation of the lipid bilayers. The bending of the monolayer will arise, to some extent, due to thermal fluctuations in the membrane, but the most dominant energy cost associated with bending arises when there is an inclusion, such as a peptide, in the membrane. Hydrophobic mismatch occurs when the hydrophobic region of the peptide is larger, or smaller, than the bilayer thickness, which causes each monolayer leaflet to distort in order to ensure that the entire hydrophobic region of the peptide is contained within the hydrophobic core of the membrane. These local membrane distortions can result in a long-range interaction between the peptides.

The free energy per amphiphile of a monolayer can be written as [24, 45–47]:

$$f(u, a_L) = \gamma a_L + G(u) + K(a_L) (\nabla^2 u - \kappa(a_L))^2, \quad (2)$$

where γ is the surface tension between the aqueous media and the hydrophobic amphiphile tails, and $G(u)$ a compression-expansion term of the amphiphiles. The thickness of the membrane, u , and the area per amphiphile molecule, a_L , are functions of the distance, r , with respect to the inclusion, *i.e.*, $u(r)$ and $a_L(r)$, and are related by an incompressibility condition to keep the lipid volume constant. The other terms stem from bending of the monolayer indicated by the local monolayer curvature $\nabla^2 u(r)$. $K(a_L)$ is the bending stiffness per molecule, so that $K(a_L) (\nabla^2 u)^2$ represents the energy related to bending the leaflet. The last term corresponds to the spontaneous curvature of the monolayer, where $\kappa(a_L)$ is the spontaneous curvature per molecule. The spontaneous curvature mainly depends on structural parameters, such as the composition of the membrane. It plays, however, an important role for the magnitude and the character of the lipid mediated interaction.

Using Equation (2), the membrane perturbation profile and the membrane-induced interactions between an array of inclusions embedded in a two-dimensional membrane have been calculated [45, 48, 49], and are sketched in Figure 11. In the case of small or vanishing spontaneous curvature, the global energy minimum is obtained at $r = 0$, which favours aggregation. A metastable, dispersed

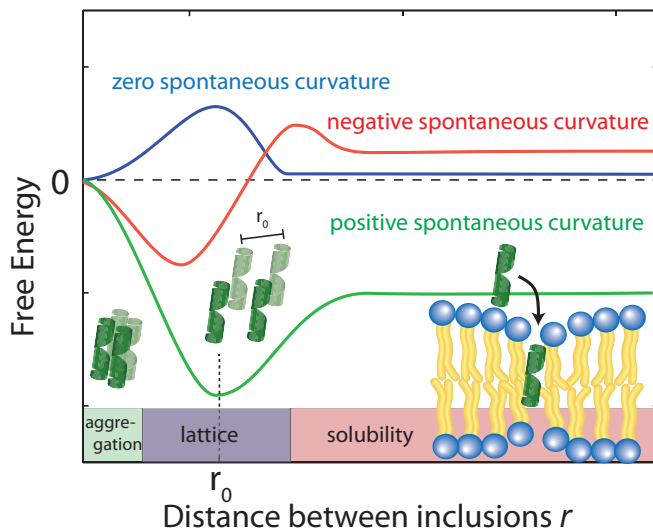


FIG. 11. Schematics of the free energy profiles for lipids with zero, positive and negative spontaneous curvature.

state exists, separated from the aggregated state by an energy barrier.

Aggregation becomes unfavourable for nonzero spontaneous curvature (positive or negative) and the energy becomes minimal at a finite spacing (r_0) between inclusions [24]. In this state the peptides are expected to arrange on a regular lattice, as for instance observed in the case of purple membrane [22]. The energy at $r \rightarrow \infty$ is a measure of the energy related to insertion of the peptide into the bilayer. If this energy is negative peptides spontaneously embed in the bilayers. In the case of $A\beta_{25-35}$, the peptide is shorter than the bilayer thickness, such that a positive spontaneous curvature favours peptide insertion.

However, POPC was reported to have a small, negative [50] spontaneous curvature, while DMPS has a small positive spontaneous curvature. Using literature values, the total spontaneous curvature of the 0.97:0.03 mix can be calculated to $J_0^{mix} = \sum_i x_i J_0^i = 0.97 \times (-0.022) \text{ nm}^{-1} + 0.03 \times (+0.068) \text{ nm}^{-1} = -0.019 \text{ nm}^{-1}$ [50]. The system is, thus, best described by the energy profile of a small spontaneous curvature in Figure 11 and the global energy minimum in this case is the aggregated state at $r = 0$. There is an energy barrier to the inclusion of the peptides into the bilayer. Once embedded, the peptides first stay in the metastable, dispersed state. It seems that the energy barrier between local and global minimum can be overcome at higher peptide concentrations: the total energy cost increases with the number of inclusions such that the free energy can be minimized by minimizing the number of membrane distortions. While the dispersed state is stable at low concentrations, peptides start to aggregate beyond a threshold concentration. From the experiments, the critical $A\beta_{25-35}$ peptide concentration in POPC is between 3 and 10 mol%.

All-atom molecular dynamics (MD) simulations [51–

53] provide microscopic details of the corresponding structure: The lipid density next to the edge of a peptide is lower than its bulk value. This depletion layer is followed by a crowded region with high lipid density. The spontaneous curvature of the monolayer determines the shape of the membrane deformation profile. The perturbation length, *i.e.*, the distance at which the membrane returns to its undistorted equilibrium thickness, is determined by compressibility and bending energy. In the computer simulations, this lateral perturbation of the lipid density was found to extend up to 25 Å from the edge of a small (cylindrical) inclusion with a radius of 5 Å, comparable to the size of the $A\beta$ peptide. The corresponding distance between inclusions of 60 Å corresponds to about 6 molecular distances, in reasonable agreement with our Monte Carlo simulations.

The Monte Carlo simulations confirm that in order to reproduce the experimental findings (no aggregates formed at low peptide concentrations and cluster size is independent of peptide concentration) a long-ranged attractive interaction between peptides is necessary. A range of 10 molecular distances provided a good agreement with the experimental observations. While a direct, short-ranged peptide-peptide interaction leads to cluster formation at all peptide concentrations, truly long-range interactions would lead to an increasing cluster size, in contradiction to the experiments.

4.2. Peptide conformations and properties of $A\beta_{25-35}$ -aggregates

Monomeric, single peptides were found in α -helical states when embedded in anionic membranes at low peptide concentrations [12, 18]. There is no sign of aggregates in the microscopy images and no additional signals in the X-ray diffraction pattern at 3 mol% peptide. We note that peptides often organize in bundles, whose structure is dominated by α -helical coiled-coils [54–58]. Coiled coils consist of α -helices wound together to form a ropelike structure stabilized by hydrophobic interactions. The main features of this motif is a ~ 9.5 Å (corresponding to $q_{\parallel} \sim 0.6 \text{ \AA}^{-1}$) equatorial reflection corresponding to the spacing between adjacent coiled-coils and a ~ 5.0 Å meridional reflection (corresponding to $q_z \sim 1.25 \text{ \AA}^{-1}$) corresponding to the superhelical structure of α -helices twisting around each other within coiled-coils [59–61]. The absence of those signals is indicative that peptides embed as monomers at low concentrations.

Aggregates were observed to form at peptide concentrations of 10 and 20 mol% and signals of cross- β -sheets were observed in the X-ray diffraction patterns. The cross- β motif is found in the spine of amyloid fibrils [1, 7], where the elementary β -strand building blocks assemble into larger structures through cross- β steric zippers. Cross- β sheets have been reported in short residue peptides [7], comparable to the length of $A\beta_{25-35}$.

It has been observed previously that amyloid- β_{1-42}

624 and amyloid- β_{25-35} peptides undergo a conformational
625 change from α -helical to β -sheet structures in the pres-
626 ence of lipid membranes [62]. The process behind β -sheet
627 formation likely takes place in several steps. In a first
628 step, the peptide makes contact with the membrane and
629 aligns parallel to the membrane, before stronger bonds
630 form and the peptide is embedded into the hydrocar-
631 bon core [63–66]. From molecular dynamics computer
632 simulations, α -helical peptides start to form small dy-
633 namical clusters of 4–6 peptides at low peptide concen-
634 trations [25]. We note that as these cluster are small and
635 transient structures, they would be difficult to observe
636 in X-ray experiments. The transition into β -sheet struc-
637 tures inside of the hydrophobic core is then the result
638 of (1) the hydrophobic effect and (2) a reduced confor-
639 mational entropy of the peptide chains [67]. Hydrophobic
640 side chains orient towards the hydrophobic lipid acyl
641 chains and reduction of the conformational freedom even-
642 tually promotes formation of β -sheets at higher peptide
643 concentrations.

644 The amyloid literature typically distinguishes between
645 the formation of a nucleus and eventually the growth
646 of amyloid fibres [1]. While the growth of the fibres ap-
647 pears to be somewhat understood, the formation of nuclei
648 seems to be less well understood. While fibres are typ-
649 ically found in the extracellular space, our experiments
650 provide plausible evidence that bilayers provide a site for
651 peptide aggregation and nuclei formation inside of the bi-
652 layers. In this particular mechanism growth of the nuclei
653 would occur by lateral attachment of further peptides.

5. CONCLUSION

655 Synthetic anionic membranes were fabricated and ag-
656 gregation of amyloid- β_{25-35} peptides into cross- β sheets
657 was observed and investigated using optical microscopy,
658 X-ray diffraction and computer modelling. Unsaturated
659 zwitterionic/anionic lipid membranes made of POPC and
660 DMPS at concentrations of POPC/3 mol% DMPS con-
661 taining 0 mol%, 3 mol%, 10 mol% and 20 mol% amyloid-
662 β_{25-35} peptides were prepared. Small, $\sim 11 \mu\text{m}$ sized
663 peptide clusters were observed at peptide concentrations
664 of 10 and 20 mol%. While cluster size was found to be
665 independent of peptide concentration, cluster density in-
666 creases with peptide concentration. Peptides in peptide
667 clusters show the cross- β sheet motif.

668 Inclusion of peptides and formation of peptide aggre-
669 gates was found to lead to local distortions of the bi-
670 layers, which induces a long range interaction between
671 the peptides. The experimentally observed cluster pat-
672 terns agree well with Monte Carlo simulations of long-
673 ranged interacting peptides. This elastic interaction may
674 be driving force behind peptide aggregation and cross-
675 β sheet formation, which may serve as seeds for further
676 growth into amyloid fibrils.

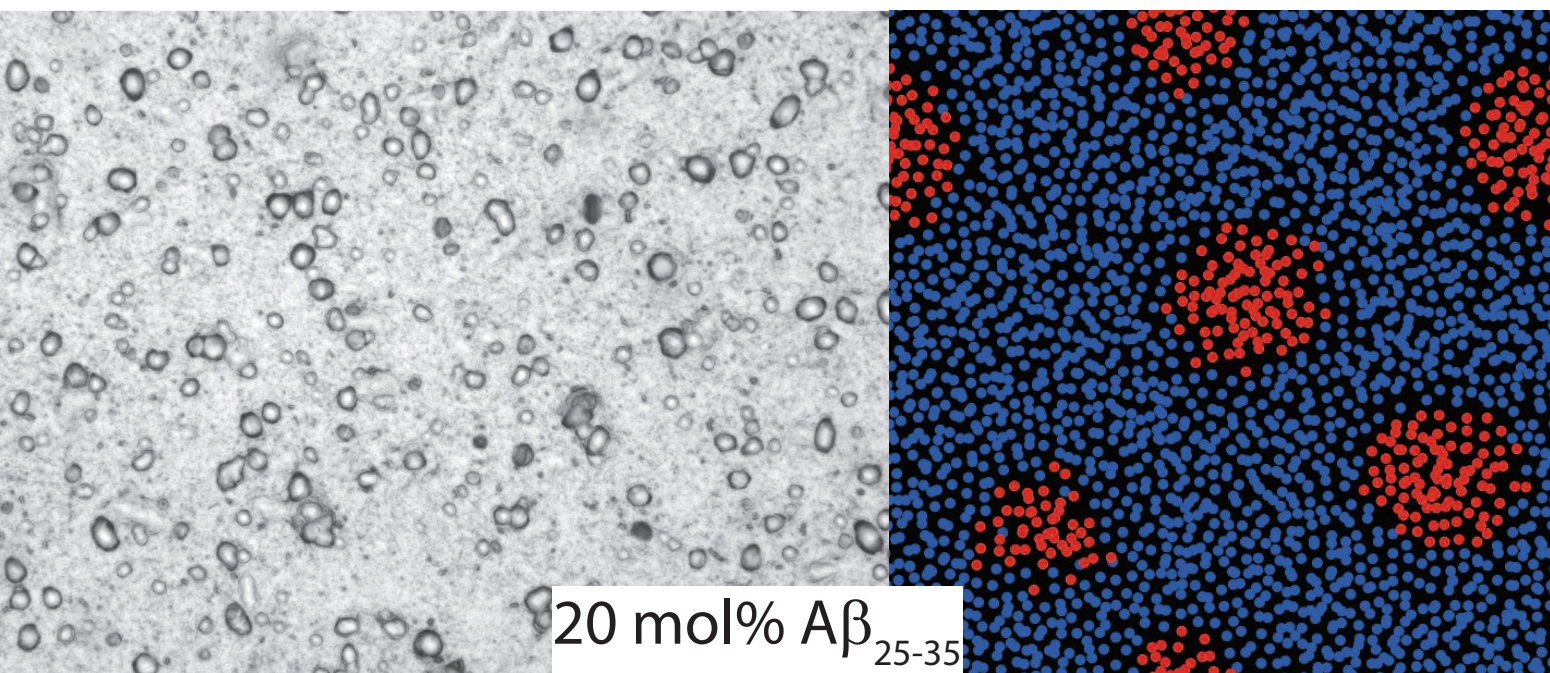
ACKNOWLEDGMENTS

678 This research was funded by the Natural Sciences and
679 Engineering Research Council of Canada (NSERC), the
680 National Research Council Canada (NRC), the Canada
681 Foundation for Innovation (CFI) and the Ontario Min-
682 istry of Economic Development and Innovation. J.T.
683 and H.D. are recipients of NSERC Undergraduate Re-
684 search Awards (USRA), R.J.A. is the recipient of an
685 NSERC PGSD scholarship, M.C.R. is the recipient of an
686 Early Researcher Award of the Province of Ontario.
687 The funders had no role in study design, data collection
688 and analysis, decision to publish, or preparation of the
689 manuscript.

-
- 690 [1] David Eisenberg and Mathias Jucker, “The amyloid state
691 of proteins in human diseases,” *Cell* **148**, 1188–1203
692 (2012).
693 [2] Barnabas James Gilbert, “The role of amyloid β in the
694 pathogenesis of alzheimer’s disease,” *Journal of Clinical*
695 *Pathology* **66**, 362–366 (2013).
696 [3] Andrew J Doig and Philippe Derreumaux, “Inhibition
697 of protein aggregation and amyloid formation by small
698 molecules,” *Current Opinion in Structural Biology* **30**,
699 50–56 (2015).
700 [4] Bernd Bohrmann, Karlheinz Baumann, Jörg Benz,
701 Françoise Gerber, Walter Huber, Frédéric Knoflach,
702 Jürg Messer, Krisztina Oroszlan, Robert Rauchenberger,
703 Wolfgang F Richter, *et al.*, “Gantenerumab: a novel hu-
704 man anti- $\alpha\beta$ antibody demonstrates sustained cerebral
705 amyloid- β binding and elicits cell-mediated removal of
706 human amyloid- β .” *Journal of Alzheimer’s Disease* **28**,
707 49–69 (2011).
708 [5] Lin Jiang, Cong Liu, David Leibly, Meytal Landau, Min-
709 glei Zhao, Michael P Hughes, and David S Eisenberg,
710 “Structure-based discovery of fiber-binding compounds
711 that reduce the cytotoxicity of amyloid β ,” *eLife* **2**,
712 e00857 (2013).
713 [6] Della C David, Noah Ollikainen, Jonathan C Trinidad,
714 Michael P Cary, Alma L Burlingame, and Cynthia
715 Kenyon, “Widespread protein aggregation as an inherent
716 part of aging in *c. elegans*,” *PLOS Biology* **8**, e1000450
717 (2010).
718 [7] Anthony WP Fitzpatrick, Galia T Debelouchina, Mar-
719 vin J Bayro, Daniel K Clare, Marc A Caporini, Vikram S
720 Bajaj, Christopher P Jaroniec, Luchun Wang, Vladimir
721 Ladizhansky, Shirley A Müller, *et al.*, “Atomic structure
722 and hierarchical assembly of a cross- β amyloid fibril,”
723 *Proceedings of the National Academy of Sciences* **110**,

- 5468–5473 (2013).
- [8] Joseph T Jarrett and Peter T Lansbury, “Seeding “one-dimensional crystallization” of amyloid: a pathogenic mechanism in alzheimer’s disease and scrapie?” *Cell* **73**, 1055–1058 (1993).
- [9] María del Mar Martínez-Senac, José Villalán, and Juan C. Gómez-Fernández, “Structure of the alzheimer β -amyloid peptide (25-35) and its interaction with negatively charged phospholipid vesicles,” *European Journal of Biochemistry* **265**, 744–753 (1999).
- [10] Elena Maltseva and Gerald Brezesinski, “Adsorption of amyloid β (1-40) peptide to phosphatidylethanolamine monolayers,” *ChemPhysChem* **5**, 1185–1190 (2004).
- [11] Garima Thakur, Miodrag Micic, and Roger M Leblanc, “Surface chemistry of alzheimer’s disease: a langmuir monolayer approach,” *Colloids and Surfaces B: Biointerfaces* **74**, 436–456 (2009).
- [12] Hui-Hsu Gavin Tsai, Jian-Bin Lee, Sheng-Shiuan Tseng, Xiao-An Pan, and Yuan-Ci Shih, “Folding and membrane insertion of amyloid- β (25–35) peptide and its mutants: Implications for aggregation and neurotoxicity,” *Proteins: Structure, Function, and Bioinformatics* **78**, 1909–1925 (2010).
- [13] Marc-Antoine Sani, John D Gehman, and Frances Separovic, “Lipid matrix plays a role in $\alpha\beta$ fibril kinetics and morphology,” *FEBS letters* **585**, 749–754 (2011).
- [14] Francis Hane, Elizabeth Drolle, Ravi Gaikwad, Erin Faught, and Zoya Leonenko, “Amyloid- β aggregation on model lipid membranes: An atomic force microscopy study,” *Journal of Alzheimer’s Disease* **26**, 485–494 (2011).
- [15] Hao Ding, Joseph A Schauerte, Duncan G Steel, and Ari Gafni, “ β -amyloid (1–40) peptide interactions with supported phospholipid membranes: A single-molecule study,” *Biophysical Journal* **103**, 1500–1509 (2012).
- [16] Hasna Ahyayauch, Michal Raab, Jon V. Busto, Nagore Andraka, José-Luis R. Arrondo, Massimo Masserini, Igor Tvaroska, and Félix M. Goni, “Binding of β -amyloid (1-42) peptide to negatively charged phospholipid membranes in the liquid-ordered state: Modeling and experimental studies,” *Biophysical Journal* **103**, 453 – 463 (2012).
- [17] R Preston Mason, Janet D Estermyer, Jeremiah F Kelly, and Pamela E Mason, “Alzheimer’s disease amyloid β peptide 25-35 is localized in the membrane hydrocarbon core: X-ray diffraction analysis,” *Biochemical and Biophysical Research Communications* **222**, 78–82 (1996).
- [18] Hannah Dies, Laura Topozini, and Maikel C. Rheinstädter, “The interaction between amyloid- β peptides and anionic lipid membranes containing cholesterol and melatonin,” *PLOS ONE* (2014), 10.1371/journal.pone.0099124.
- [19] Silvia Dante, Thomas Hauss, and Norbert A Dencher, “ β -amyloid 25 to 35 is intercalated in anionic and zwitterionic lipid membranes to different extents,” *Biophysical Journal* **83**, 2610–2616 (2002).
- [20] Silvia Dante, Thomas Hauf, and Norbert A Dencher, “Cholesterol inhibits the insertion of the alzheimer’s peptide $\alpha\beta$ (25–35) in lipid bilayers,” *European Biophysics Journal* **35**, 523–531 (2006).
- [21] Silvia Dante, Thomas Hauss, Roland Steitz, Claudio Canale, and Norbert A. Dencher, “Nanoscale structural and mechanical effects of β -amyloid (1-42) on polymer cushioned membranes: A combined study by neutron reflectometry and {AFM} force spectroscopy,” *Biochimica et Biophysica Acta (BBA) - Biomembranes* **1808**, 2646 – 2655 (2011).
- [22] Maikel C. Rheinstädter, Karin Schmalzl, Kathleen Wood, and Dieter Strauch, “Protein-protein interaction in purple membrane,” *Physical Review Letters* **103**, 128104 (2009).
- [23] Ignacio Casuso, Pierre Sens, Felix Rico, and Simon Scheuring, “Experimental evidence for membrane-mediated protein-protein interaction,” *Biophysical Journal* **99**, L47–L49 (2010).
- [24] Clare L. Armstrong, Erik Sandqvist, and Maikel C. Rheinstädter, “Protein-protein interactions in membranes,” *Protein and Peptide Letters* **18**, 344–353 (2011).
- [25] Martina Pannuzzo, Antonio Raudino, Danilo Milardi, Carmelo La Rosa, and Mikko Karttunen, “ α -helical structures drive early stages of self-assembly of amyloidogenic amyloid polypeptide aggregate formation in membranes,” *Scientific Reports* **3** (2013).
- [26] Shachi Katira, Kranthi K Mandadapu, Suriyanarayanan Vaikuntanathan, Berend Smit, and David Chandler, “The order-disorder phase transition in lipid bilayers mediates a force for assembly of transmembrane proteins,” *arXiv preprint arXiv:1506.04298* (2015).
- [27] Shu-Chuan Jao, Kan Ma, Joseph Talafous, Ron Orlando, and Michael G Zagorski, “Trifluoroacetic acid pretreatment reproducibly disaggregates the amyloid β -peptide,” *Amyloid* **4**, 240–252 (1997).
- [28] Thalia T. Mills, Gilman E. S. Toombes, Stephanie Tristram-Nagle, Detlef-M. Smilgies, Gerald W. Feigenson, and John F. Nagle, “Order parameters and areas in fluid-phase oriented lipid membranes using wide angle x-ray scattering,” *Biophysical Journal* **95**, 669–681 (2008).
- [29] Michael S Jablin, Kiyotaka Akibori, and John F. Nagle, “Experimental support for tilt-dependent theory of biomembrane mechanics,” *Physical Review Letters* **113**, 248102 (2014).
- [30] Uri Wilensky, “Netlogo,” Center for Connected Learning and Computer-Based Modeling, Northwestern University, <http://ccl.northwestern.edu/netlogo/> (1999).
- [31] Seth Tisue and Uri Wilensky, “Netlogo: A simple environment for modeling complexity,” in *International conference on complex systems* (2004) pp. 16–21.
- [32] Peter A Leventis and Sergio Grinstein, “The distribution and function of phosphatidylserine in cellular membranes,” *Annual Review of Biophysics* **39**, 407–427 (2010).
- [33] Georg Pabst, Norbert Kučerka, Mu-Ping Nieh, Maikel C. Rheinstädter, and J. Katsaras, “Applications of neutron and x-ray scattering to the study of biologically relevant model membranes,” *Chemistry and Physics of Lipids* **163**, 460 – 479 (2010).
- [34] Giovanna Fragneto and Maikel Rheinstädter, “Structural and dynamical studies from bio-mimetic systems: an overview,” *Comptes Rendus Physique* **8**, 865–883 (2007).
- [35] Clare L. Armstrong, Drew Marquardt, Hannah Dies, Norbert Kučerka, Zahra Yamani, Thad A. Harroun, John Katsaras, An-Chang Shi, and Maikel C. Rheinstädter, “The observation of highly ordered domains in membranes with cholesterol,” *PLOS ONE* **8**, e66162 (2013).
- [36] Maikel C. Rheinstädter, Tilo Seydel, Franz Demmel, and Tim Salditt, “Molecular motions in lipid bilayers studied by the neutron backscattering technique,” *Phys. Rev. E* **71**, 061908 (2005).

- [37] Maikel C. Rheinstädter, Tilo Seydel, and Tim Salditt, “Nanosecond molecular relaxations in lipid bilayers studied by high energy resolution neutron scattering and in-situ diffraction,” *Phys. Rev. E* **75**, 011907 (2007).
- [38] Laura Toppozini, Clare L. Armstrong, Martin D. Kaye, Madhusudan Tyagi, Timothy Jenkins, and Maikel Rheinstädter, “Hydration water freezing in single supported lipid bilayers,” *ISRN Biophysics* **2012**, 520307 (2012).
- [39] Laura Toppozini, Felix Roosen-Runge, Robert I Bewley, Robert M Dalgliesh, Toby Perring, Tilo Seydel, Henry R Glyde, Victoria García Sakai, and Maikel C Rheinstädter, “Anomalous and anisotropic nanoscale diffusion of hydration water molecules in fluid lipid membranes,” *Soft Matter* (2015).
- [40] John Katsaras, Velayudhan A. Raghunathan, Erick J. Dufourc, and Jean Dufourcq, “Evidence for a two-dimensional molecular lattice in subgel phase dppc bilayers,” *Biochemistry* **34**, 4684–4688 (1995).
- [41] Velayudhan A. Raghunathan and J. Katsaras, “Structure of the l'_c phase in a hydrated lipid multilamellar system,” *Physical Review Letters* **74**, 4456–4459 (1995).
- [42] Matthew A. Barrett, Songbo Zheng, Golnaz Roshankar, Richard J. Alsop, Randy K.R. Belanger, Chris Huynh, Norbert Kučerka, and Maikel C. Rheinstädter, “Interaction of aspirin (acetylsalicylic acid) with lipid membranes,” *PLOS ONE* **7**, e34357 (2012).
- [43] Maikel C. Rheinstädter, Wolfgang Häußler, and Tim Salditt, “Dispersion relation of lipid membrane shape fluctuations by neutron spin-echo spectrometry,” *Physical Review Letters* **97**, 048103 (2006).
- [44] Clare L. Armstrong, Wolfgang Häußler, Tilo Seydel, John Katsaras, and Maikel C. Rheinstädter, “Nanosecond lipid dynamics in membranes containing cholesterol,” *Soft Matter* **10**, 2600–2611 (2014).
- [45] Helim Aranda-Espinoza, A Berman, Nily Dan, Philip Pincus, and Sam Safran, “Interaction between inclusions embedded in membranes.” *Biophysical Journal* **71**, 648 (1996).
- [46] Wolfgang Helfrich, “Elastic properties of lipid bilayers: theory and possible experiments,” *Zeitschrift für Naturforschung C* **28**, 693–703 (1973).
- [47] Robijn Bruinsma and Philip Pincus, “Protein aggregation in membranes,” *Current Opinion in Solid State and Materials Science* **1**, 401–406 (1996).
- [48] Nily Dan, Philip Pincus, and Sam A. Safran, “Membrane-induced interactions between inclusions,” *Langmuir* **9**, 2768–2771 (1993).
- [49] Nily Dan, A Berman, Philip Pincus, and Sam A. Safran, “Membrane-induced interactions between inclusions,” *Journal de Physique II* **4**, 1713–1725 (1994).
- [50] Benjamin Kollmitzer, Peter Heftberger, Michael Rappolt, and Georg Pabst, “Monolayer spontaneous curvature of raft-forming membrane lipids,” *Soft Matter* **9**, 10877–10884 (2013).
- [51] Patrick Lagüe, Martin J Zuckermann, and Benoît Roux, “Protein inclusion in lipid membranes: a theory based on the hypernetted chain integral equation,” *Faraday Discussions* **111**, 165–172 (1999).
- [52] Patrick Lagüe, Martin J Zuckermann, and Benoît Roux, “Lipid-mediated interactions between intrinsic membrane proteins: a theoretical study based on integral equations,” *Biophysical Journal* **79**, 2867–2879 (2000).
- [53] Patrick Lagüe, Martin J Zuckermann, and Benoît Roux, “Lipid-mediated interactions between intrinsic membrane proteins: dependence on protein size and lipid composition,” *Biophysical Journal* **81**, 276–284 (2001).
- [54] Linus Pauling and Robert B Corey, “Two hydrogen-bonded spiral configurations of the polypeptide chain,” *Journal of the American Chemical Society* **72**, 5349–5349 (1950).
- [55] Nicole Pinto, Fei-Chi Yang, Atsuko Negishi, Maikel C. Rheinstädter, Todd E. Gillis, and Douglas S. Fudge, “Self-assembly enhances the strength of fibers made from vimentin intermediate filament proteins,” *Biomacromolecules* **15**, 574–581 (2014).
- [56] Fei-Chi Yang, Robert D. Peters, Hannah Dies, and Maikel C. Rheinstädter, “Hierarchical, self-similar structure in native squid pen,” *Soft Matter* **10**, 5541–5549 (2014).
- [57] Fei-Chi Yang, Yuchen Zhang, and Maikel C Rheinstädter, “The structure of peoples hair,” *PeerJ* **2**, e619 (2014).
- [58] Yuchen Zhang, Richard J Alsop, Asfia Soomro, Fei-Chi Yang, and Maikel C Rheinstädter, “Effect of shampoo, conditioner and permanent waving on the molecular structure of human hair,” *PeerJ* (2015).
- [59] Francis H.C. Crick, “Is α -keratin a coiled coil?” *Nature* **170**, 882 – 883 (1952).
- [60] C Cohen and DA Parry, “ α -helical coiled coils: more facts and better predictions,” *Science* **263**, 488–489 (1994).
- [61] Andrei N Lupas and Markus Gruber, “The structure of α -helical coiled coils,” *Advances in protein chemistry* **70**, 37–38 (2005).
- [62] Angelo Accardo, Victoria Shalabaeva, Marine Cotte, Manfred Burghammer, Roman Krahné, Christian Riekell, and Silvia Dante, “Amyloid β peptide conformational changes in the presence of a lipid membrane system,” *Langmuir* **30**, 3191–3198 (2014).
- [63] Huey W Huang, “Action of antimicrobial peptides: two-state model,” *Biochemistry* **39**, 8347–8352 (2000).
- [64] Donald M Engelman, Yang Chen, Chen-Ni Chin, A Rachael Curran, Ann M Dixon, Allison D Dupuy, Albert S Lee, Ursula Lehnert, Erin E Matthews, Yana K Reshetnyak, *et al.*, “Membrane protein folding: beyond the two stage model,” *Febs Letters* **555**, 122–125 (2003).
- [65] Matthias Heyden, J Alfredo Freites, Martin B Ulmschneider, Stephen H White, and Douglas J Tobias, “Assembly and stability of α -helical membrane proteins,” *Soft Matter* **8**, 7742–7752 (2012).
- [66] Chang-Chun Lee, Yen Sun, and Huey W Huang, “Membrane-mediated peptide conformation change from α -monomers to β -aggregates,” *Biophysical Journal* **98**, 2236–2245 (2010).
- [67] Ana Nikolic, Stéphanie Baud, Sarah Rauscher, and Régis Pomès, “Molecular mechanism of β -sheet self-organization at water-hydrophobic interfaces,” *Proteins: Structure, Function, and Bioinformatics* **79**, 1–22 (2011).



$A\beta_{25-35}$

